Ocean Engineering 290 (2023) 116296

Contents lists available at ScienceDirect

Ocean Engineering

journal homepage: www.elsevier.com/locate/oceaneng

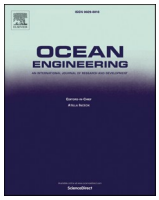

Estimation of probability of large roll angle with envelope peaks over threshold method

Bradley Campbell [a], Vadim Belenky [a,*], Vladas Pipiras [b], Kenneth Weems [a], Themistoklis P. Sapsis [c]

[a] David Taylor Model Basin, NSWCCD, USA
[b] University of North Carolina, Chapel Hill, USA
[c] Massachusetts Institute of Technology, USA

ARTICLE INFO

Handling Editor: Prof. A.I. Incecik

Keywords:
Statistic of extremes
Large roll
Physics-informed statistical models
EPOT

ABSTRACT

The development and application of the Envelope Peak-over-Threshold (EPOT) method is summarized for the roll motion of a ship in irregular waves. The method is based on the conventional Peak-over-Threshold (POT) method, but uses an envelope of the peaks for declustering the data. As suggested by a reduced-order model, a power-law tail should be applicable for the peaks of roll motions, which allows the introduction of physical considerations into the statistical model. A data-driven Generalized Pareto distribution (GPD) is applied to study the behavior of the shape parameter on large-volume samples in order to confirm the theoretical prediction of the tail structure. The physics-informed statistical model approximates data above a suitable threshold with a Pareto distribution, while the threshold is determined with a prediction error criterion. An example is included, where extrapolations with GPD are compared to the physics-informed model.

1. Introduction

The probability of the occurrence of a large roll angle in irregular seas is a useful characterization of the dynamic stability of a ship. The calculation of this probability, however, is far from trivial. The linear roll restoring, implicit in frequency domain tools, makes them unsuitable for the task, so time-domain simulations are required. An analysis using engineering-level tools like the Large Amplitude Motions Program (LAMP) (Shin et al., 2003) and TEMPEST (Belknap and Reed, 2019) typically generates, at best, tens of hours of simulation time history for each combination of loading, operational and sea conditions. Large roll angles are expected to be rare, far too rare to be estimated through direct counting with such tools. In order to estimate the probability of an event beyond the duration of practical simulations, an extrapolation method is required.

The objective of statistical extrapolation is, therefore, to characterize a likelihood of the exceedance of a large roll angle ϕ^* without necessarily observing such large angles. The angle ϕ^* is further referred to as a "target" of extrapolation. The value of ϕ^* may depend on specific risk or criteria being evaluated. The interim guidance for the second generation IMO intact stability criteria uses exceedance of 40° as a failure event for direct stability assessment, see paragraph 3.2.1.1 in MSC.1/Circ.1627 (IMO, 2020).

The most natural way to perform such an extrapolation is to approximate the distribution of roll motions. Belenky et al. (2023) presents a review of the state of the art and historical development of approximates of the distribution of roll motion. To characterize a large roll angle, the approximation of distribution of roll motions above a certain value, i.e. a tail of that distribution, may be sufficient. To formulate the problem, recall the definition of cumulative distribution function (CDF) of a random variable, say, a peak or instantaneous value of roll motions in irregular waves. It is defined as a probability that a random variable X takes a value less or equal to x, and can be expressed in the more commonly used probability density function (PDF), which is a derivative of the CDF:

$$\mathrm{CDF}(x) = P(X \le x) = \int_0^x \mathrm{PDF}(z)dz. \tag{1}$$

The tail of a distribution relates to the exceedance of a certain "threshold" value u, which is an event complimentary to the one, described in (1):

* Corresponding author.
E-mail address: vadim.belenky@navy.mil (V. Belenky).

https://doi.org/10.1016/j.oceaneng.2023.116296
Received 24 May 2023; Received in revised form 4 November 2023; Accepted 5 November 2023
Available online 22 November 2023
0029-8018/Published by Elsevier Ltd.

$$P(X > u) = 1 - \mathrm{CDF}(u) = \int_u^{\infty} \mathrm{PDF}(z)dz. \tag{2}$$

The approximation of a tail, as shown in Fig. 1, may be a simpler problem than the approximation of the entire distribution. Once the tail of the distribution is approximated such that it can be evaluated at the target value, the extrapolation problems is solved.

The threshold value u is a beginning of the tail of distribution. For the tail to be fitted from data, this threshold must be within the available data. The probability of exceedance of the threshold is estimated as:

$$\widehat{P}(\phi > u) = \frac{m}{n}, \tag{3}$$

where m is the number of observed roll angles above the threshold and n is the total number of data points available. A diacritical sign "hat" $\widehat{\ }$ above a letter means that the value is estimated from the data and has statistical uncertainty caused by the finite volume of the sample.

In principle, any function can be used to approximate the tail of a distribution, if a normalization condition is satisfied. When fitting a tail, rather than a complete distribution, to available data, one needs to ensure the normalization condition is still satisfied and the area under the PDF equals unity.

The estimate of the probability of exceedance of the target value is expressed as:

$$\widehat{P}(\phi > \phi^*) = \frac{1}{N_{tl}}\widehat{P}(\phi > u)\int_{\varphi^*}^{\infty} f_{tl}(\phi)d\phi, \tag{4}$$

where N_{tl} is a normalizing coefficient for the approximated tail:

$$N_{tl} = \int_u^{\infty} f_{tl}(\phi)d\phi. \tag{5}$$

If a theoretical PDF is used to approximate the tail and it supports the range $[u;\infty)$, $N_{tl} = 1$. Then,

$$\widehat{P}(\phi > \phi^*) = \widehat{P}(\phi > u)\int_{\phi^*}^{\infty} PDF_{tl}(\phi)d\phi = \widehat{P}(\phi > u)(1 - CDF_{tl}(\phi^*)). \tag{6}$$

If the characterization of the likelihood of a large angle needs to account for the time of exposure, the objective of the extrapolation is the estimation of a rate of exceedance of the target. Direct stability assessment within the second generation IMO intact stability criteria does include exposure time considerations and uses an estimate of the rate of failures (exceedances of 40° on either side) to judge the dynamic stability of a ship.

When a probability distribution with support $[u;\infty)$ is used to approximate a tail, the extrapolated estimate of rate is expressed as:

$$\widehat{r}_{\phi^*} = \widehat{r}_u\int_{\phi^*}^{\infty} PDF_{tl}(\phi)d\phi = \widehat{r}_u(1 - CDF_{tl}(\phi^*)). \tag{7}$$

where $\widehat{r}_u$ is an estimate of the crossing of the threshold u. Essentially the term $(1 - CDF_{tl}(\phi^*))$ shows how many of the exceedances of the threshold u will end up exceeding the target ϕ^* as well. The rate of exceedances of the threshold $\widehat{r}_u$ can be estimated as

$$\widehat{r}_u = \frac{\widehat{P}(\phi > u)}{T}, \tag{8}$$

where T is the time of exposure, i.e. total time of available data. There is more than one way to estimate a rate of exceedance from available data; these techniques are sometimes referred as "direct counting". More information is available from Wandji et al. (2024).

Generally, the approximation of the tail can be completely data driven, as the distribution of the largest value in a sample of independent data points tends towards a generalized extreme value distribution (GEV) and does not depend on the actual distribution of the variable (or underlying distribution). Three particular cases of the GEV are: Gumbel, Fréchet and Weibull distributions. This is the essence of the first extreme value theorem, which is also known as the Fisher-Tippet-Gnedenko theorem. The second extreme value theorem, also known as the Pickands-Balkema-de Haan theorem, states that a distribution of independent data over a large-enough threshold u can be approximated with Generalized Pareto distribution (GPD), e.g. see Coles (2001):

$$\mathrm{PDF}_{GPD}(x) = \begin{cases} \frac{1}{\sigma}\exp\left(-\frac{x-u}{\sigma}\right) \text{ if } \xi = 0 \\ \frac{1}{\sigma}\left(1 + \xi\frac{x-u}{\sigma}\right)^{-(1+1/\xi)} \text{ if } \xi \neq 0,\ \xi\frac{x-u}{\sigma} > -1 \\ 0 \text{ otherwise} \end{cases} \tag{9}$$

where ξ is the shape parameter and σ is the scale parameter.

From equation (9), a distribution with a negative shape parameter has a right bound at $x = u - \sigma/\xi$. Such a tail is referred to as "light". In the case of a positive shape parameter, the tail is infinite and is referred to as "heavy". For $\xi = 0$, the tail is also infinite but always below a heavy tail. The $\xi = 0$ case serves as a border between the heavy and light tails and is referred to as "exponential". Normal and Rayleigh distributions have exponential tails.

GPD was formulated for the approximation of tails by Pickands (1975), and is the principal tool in the Peak-over-Threshold (POT) method. To fit the GPD, several candidate thresholds are selected and the shape and scale parameters are estimated from the data above each threshold. Some convergence criteria are applied to select the "large-enough" threshold from the candidates. Data points for the POT method application have to be independent, as equation (9) is formulated for independent data.

The first attempt to use the POT approach for the peaks of roll motion utilized a Weibull distribution rather than GPD (Campbell and Belenky, 2010, 2010a). An envelope was used to ensure the independence of the data, giving a name to the technique – Envelope Peak over Threshold (EPOT). The concept of a threshold was interpreted from a physical standpoint; as a way to separate the domain where the influence of nonlinearity is significant. This led to the formulation of the "principle of separation" (e.g. Belenky et al., 2012). The complex problem of the extrapolation of ship motions is separated in two simpler problems: *non-rare* and *rare*. The non-rare problem is focused on observable quantities and can be handled with quasi-linear methods as its domain is characterized by weak nonlinearity. The rare problem is relevant to the strongly nonlinear response. Performing the extrapolation on only the large-amplitude response emphasizes the nonlinear effect. A similar approach can be found in the probabilistic decomposition-synthesis method (Mohamad et al., 2016).

The choice of the Weibull distribution for the rare problem follows its traditional application to the estimation of lifetime wave loads. The mathematical justification for the application of Weibull for both loads and motions is unclear. While the Weibull distribution is a particular case of GEV, it describes a left tail (i.e. minima). Originally, Weibull was applied to the statistics of the size of coal particles (Rosin and Rammler, 1933).

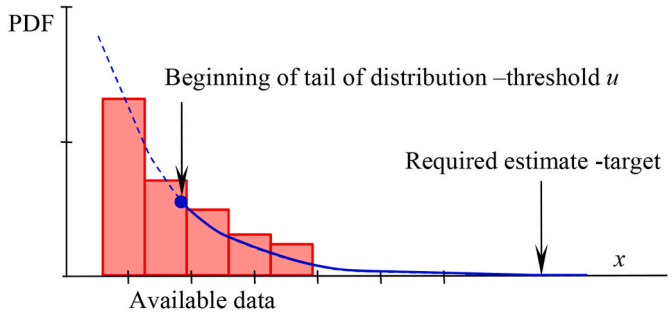

Fig. 1. Approximation of the tail of a distribution and statistical extrapolation.

The application of GPD for approximating the distribution tail for peaks of roll motions, including different aspects of estimating parameters, selecting thresholds and constructing a confidence interval, were described by the authors in Campbell et al. (2014, 2015, 2016). A methodology for the statistical validation of extrapolation methods was developed (Smith, 2019) and has been pursued using large roll motion data sets generated with a fast qualitatively-correct simulation tool (Weems and Wundrow, 2013; Weems and Belenky, 2015, 2023).

While the application of GPD has a robust mathematical background, its practical application can be challenging. The estimation of the shape parameter from a finite volume of data is a statistical procedure and its result is subject to statistical uncertainty, i.e. an estimate of the shape parameter is random number. A natural variability in the data may lead to a significantly negative estimate, which will cause the extrapolation to fail, if the extrapolation target is above the right bound. This and other challenges of practical GPD applications are described by Pipiras (2020) as well as Anastopoulos and Spyrou (2023).

These challenges may be overcome by introducing physical properties of the problem into the statistical model. Belenky et al. (2019) studied a reduced-order model of roll with piecewise linear restoring, for which an analytical solution of the distribution of peaks can be found. That distribution had a heavy tail, a result that can be applied in the statistical model to make the extrapolation more robust. Such physics-informed statistical models are the principal focus of this paper. The GPD tail approximation is also considered – for the study of behavior of the shape parameter and comparison with the physics-informed statistical model. This paper extends previous publications focusing on the method itself (Belenky et al., 2018; Weems et al., 2019), while the statistical validation of the method is covered by Campbell et al. (2023). The paper has the following structure.

- Description of the input data for EPOT
- Brief review of GPD fit
- Review of the reduced-order model for roll motions and the argument why the tail of distribution is expected to be heavy
- Observation and analysis of actual behavior of these tails for different wave heading angles
- Description of the algorithm of fitting heavy tail and comparison of results of the GPD and heavy tail extrapolation.

2. Data for EPOT extrapolation

The EPOT method was originally intended for the extrapolation of data generated by numerical simulations. The data for this paper have been taken from the validation data set described in Campbell et al. (2023), which was generated with the fast simulation tool "SimpleCode" (Weems and Wundrow, 2013; Weems and Belenky, 2015, 2023). SimpleCode incorporates a volume-based evaluation of the body-nonlinear hydrostatic and incident wave (Froude-Krylov) forces coupled with ordinary differential equation (ODE) type models for added mass, damping and other hydrodynamic forces.

The simulations were completed for the Office of Naval Research (ONR) Topsides Series tumblehome configuration (Bishop et al., 2005) with three degrees of freedom (3-DOF): heave, roll and pitch. The hull and the calm water roll restoring (GZ) curve as well as variation are depicted in Fig. 2. The loading condition had a draft 5.5 m and zero trim (even keel), while the GM value was 2.2 m. Long-crested irregular waves were represented by 240 wave components generated from a Bretschneider (1959) spectrum with a significant wave height of 9 m and modal period of 15 s, which corresponds to a high Sea State 7 or low Sea State 8. Forward speed was 6 knots in stern quartering seas with a heading of 45° (other headings were also used for the study of the shape parameter).

The data for extrapolation consisted of a series of 30-min records, with pseudo-random phases to produce independent realization of the seaway. Data variability is illustrated with three data sets, each containing 50 records.

Much of extreme value theory and the GPD (equation (9)), in particular, are applicable to independent data. Roll motions of the present configuration retain a self-dependence for about 1 min, as illustrated by the autocorrelation plot in Fig. 3a. This decorrelation time is estimated when the envelope of the estimate of autocorrelation function crosses the accepted level of significance, see Fig. 3a. With a typical zero-crossing roll period of about 10 s, each peak will be dependent on 12 or so adjacent peaks (positive and negative). To use this data for the approximation of the distribution tail with extreme value theory, the self-dependency in the data needs to be removed. This removal of self-dependency is called "declustering" and is done here with an envelope, as illustrated in Fig. 3b.

The envelope is constructed from the absolute values of roll peaks between zero-crossings and is averaged over the course of a record. The largest envelope value between two mean-level crossings is then selected for further processing. As can be seen from the example in Fig. 3b, the interval between such mean-crossing peaks is a bit more than a minute (the first mean-crossing peak is about 80 s, while the second one is at 140 s in Fig. 3b), which is roughly the decorrelation time. This declustering technique does not work well for parametric roll, as the roll motions have a long decorrelation time (up to 10 min) when parametric resonance is present (Kim et al., 2014). To perform declustering for parametric roll data, the decorrelation time has to be estimated and applied directly. Declustering with the envelope provided 1470 independent data points (roll peaks) for the data set 1, while the sample volume was 1469 and 1446 points for the data sets 2 and 3, respectively.

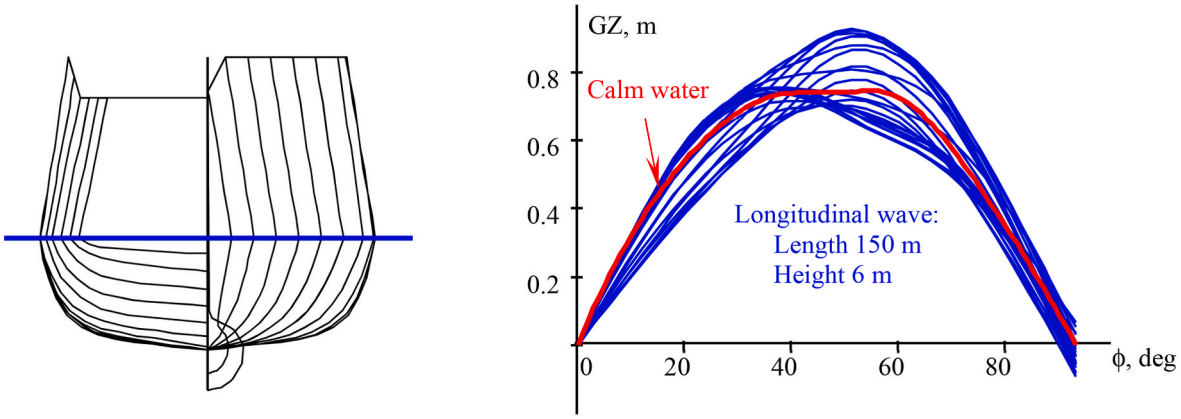

Fig. 2. Lines and GZ Curves in Calm Water and Wave of ONR Tumblehome Topside Configuration (*Bishop et al., 2005*).

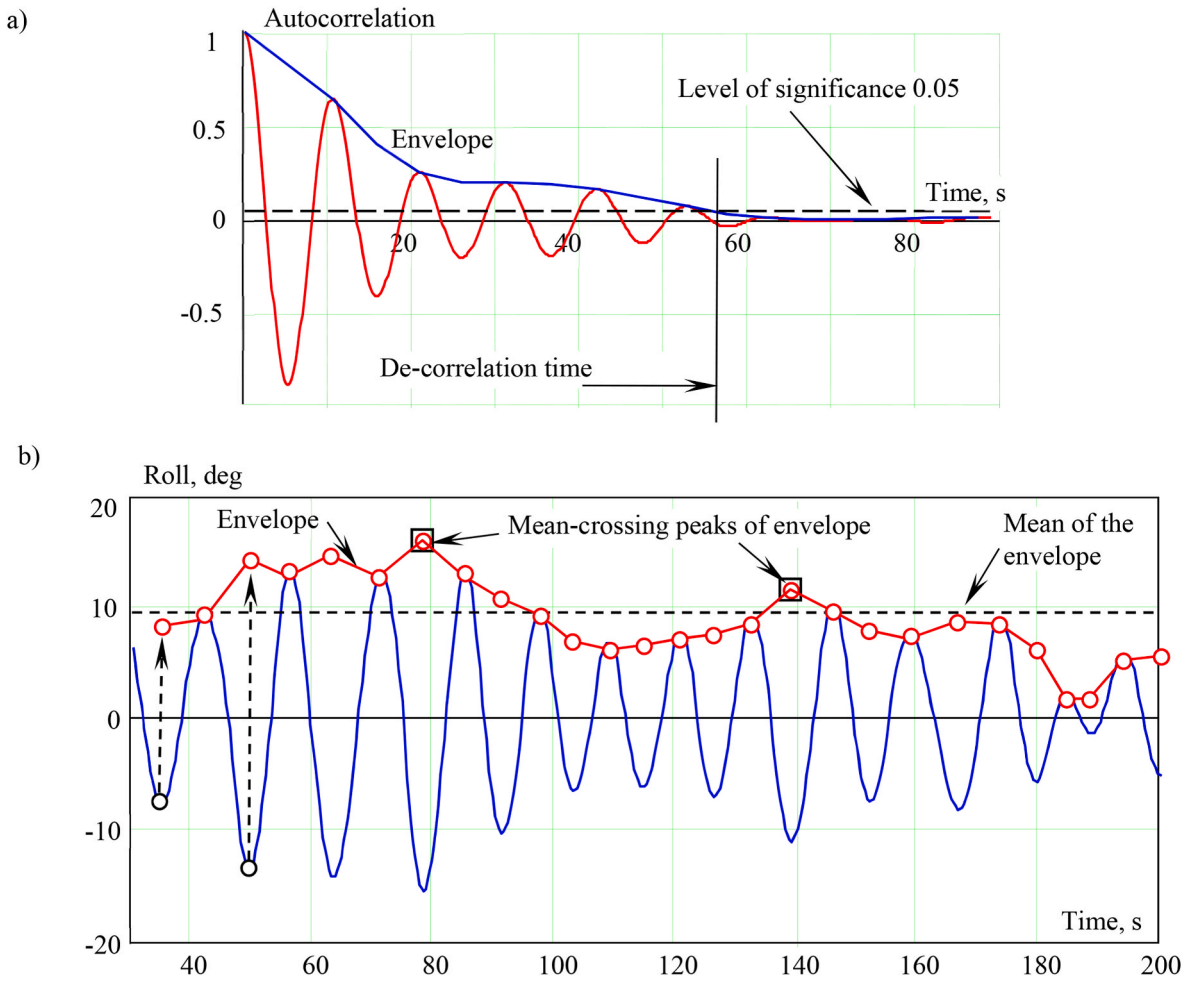

Fig. 3. (a) Decorrelation time for roll motions (b) Declustering roll motion data with the envelope.

3. Fitting the GPD

The GPD fitting procedure applied in this paper generally follows Campbell et al. (2016), with some small updates derived from a similar application for the capsizing likelihood metric in the split-time method (Belenky et al., 2023). The target value for extrapolation was set to a roll angle of 40° (an angle of stability failure in MSC.1/Circ.1627 (IMO, 2020)). The fitting involved the following calculations:

- The data were sorted in descending order and a set of candidate thresholds was selected to provide 50 data points for the highest threshold. The lowest threshold was set to have 90 % of the data points above it. Totally, 64 candidate thresholds were selected ranging from 6.9 to 16.1 deg.
- Mean values and variances of the data above each threshold were estimated. The initial guesses for the shape and scale parameters were computed with the formulae for mean value and variance of GPD. These initial guess values were used for the minimization of the negative log likelihood function reduced to one variable (which is a ratio between shape and scale parameters). The actual estimates were recovered from that minimum.
- A covariance matrix for the scale and shape parameters was computed and a confidence interval was constructed for the estimates of shape and modified scale parameter $\widehat{\sigma}_m = \widehat{\sigma} - \widehat{\xi}u$. Confidence probability was set to $P_\beta = 0.95$.
- Four methods for the threshold selections were applied. The first method was based on the stabilization of the shape parameter. A dashed line extended from a shape parameter estimate at a candidate threshold crosses all the confidence intervals of the estimate above in Fig. 4a for data set 1. Fig. 5a and Fig. 6a show stabilization of the shape parameters for data sets 2 and 3, respectively. The second method applies the same principle to the estimate of the modified scale parameter in Fig. 4b. Application of the second method for data sets 2 and 3 is illustrated in Fig. 5b and Fig. 6b. The third and fourth methods minimize the difference between the GPD and observed distribution as expressed as a cumulative distribution function (CDF). The difference is defined in terms of the distribution modes above the threshold for the third method (Fig. 4c, Fig. 5c, and Fig. 6c) or as a standard deviation for the fourth method (Fig. 4d, Fig. 5d, and Fig. 6d). The selected threshold is the largest of the four. These methods of threshold selection produce a minimum value where extreme properties may be applicable. If four different methods provide four different values, the largest among them, ensures the applicability of the extreme properties from the point of view of all four methods.
- The extrapolated estimate, its mean value and its confidence interval are computed. The latter is constructed with two methods: a "boundary" method, in which calculations are completed for the upper and lower boundaries of the parameters, accounting for their dependence, and with the CDF of the extrapolated estimate, available from Campbell et al. (2016).

The numerical results of the GPD extrapolation are summarized in Tables 1 and 2. The data sets for extrapolation were selected to demonstrate three distinctive scenarios: positive shape parameter (data set 1, Fig. 4a), negative shape parameter, the right bound above the

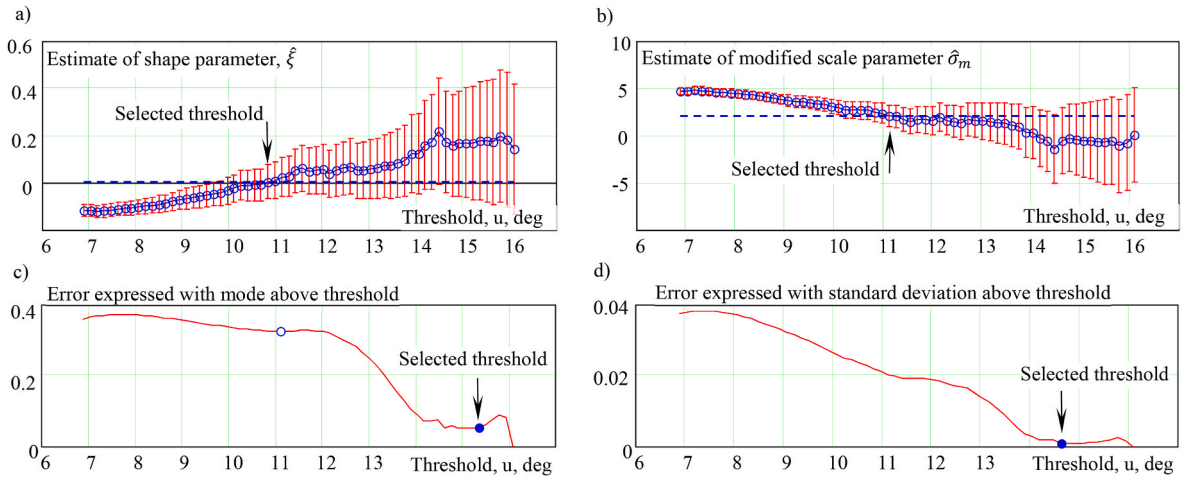

Fig. 4. Selection of threshold for GPD for data set 1 (a) stabilization of shape parameter estimate (b) stabilization of modified scale parameter (c) minimization of error expressed with mode above threshold (d) minimization of error expressed with standard deviation above threshold.

Table 1
GPD fitting results.

Data set	Volume of sample	Selected threshold, deg.	Number of data points above the threshold	Estimate of shape parameters	Right bound, deg.
1	1470	15.3	75	0.177	N/A
2	1469	11.6	399	−0.054	61.4
3	1446	9.1	776	−0.143	31.3

Table 2
Results of GPD extrapolation.

Data set	Most probable value	Mean value	"Boundary" method for confidence interval		Application of CDF for extrapolated estimate	
			low	up	low	up
1	$1.56{\cdot}10^{-3}$	$2.59{\cdot}10^{-3}$	0	0.016	0	0.013
2	$1.73{\cdot}10^{-7}$	$7.06{\cdot}10^{-6}$	0	$3.15{\cdot}10^{-4}$	0	$9.49{\cdot}10^{-5}$
3	0	$4.11{\cdot}10^{-10}$	0	$2.99{\cdot}10^{-7}$	0	$1.80{\cdot}10^{-10}$

target (data set 2, Fig. 5a) and negative shape parameter with right bound below the target (data set 3, Fig. 6a).

The behavior of the shape parameters as a function of threshold value is different for the three scenarios. The estimate of the shape parameter for data set 1 increases and stabilizes around 0.2 at a threshold of 14°, as shown in Fig. 4a. The shape parameter estimate for data set 2 settles around zero after 12°, see Fig. 5a. The data set 3 estimate stabilizes around the 12° threshold but stays negative, as shown in Fig. 6a. Such a strong influence of natural variability of the data on the behavior of the shape parameter estimates is likely a reflection of a slow convergence of the extreme value distributions.

Another notable feature is the difference between the most probable estimates (the result of substituting the estimates of the parameters into equation (1)) and the mean values (the result of integration of the PDF of the extrapolated estimates), see Table 2. While the difference between the mean and most probable values is relatively small for the data set 1, it becomes noticeably larger for data set 2. As for the data set 3, the mean is the only non-zero value available, as the target is above the right bound, and the most probable extrapolated estimate is zero.

4. Reduced-order model for roll peaks

The significant influence of natural data variability on the estimate of shape parameter raises a natural question: are there any physical reasons

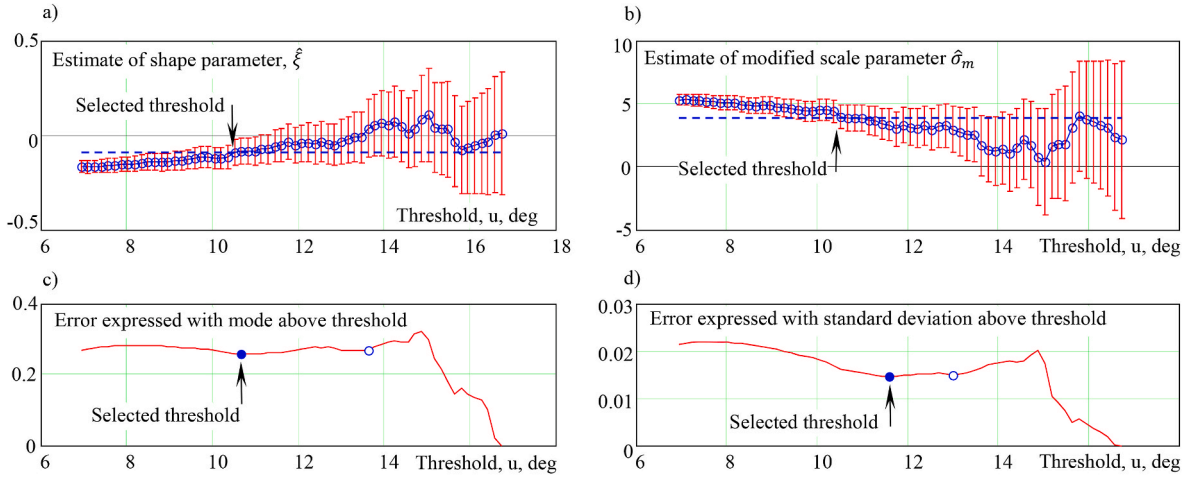

Fig. 5. Selection of threshold for GPD for data set 2 (a) stabilization of shape parameter estimate (b) stabilization of modified scale parameter (c) minimization of error expressed with mode above threshold (d) minimization of error expressed with standard deviation above threshold.

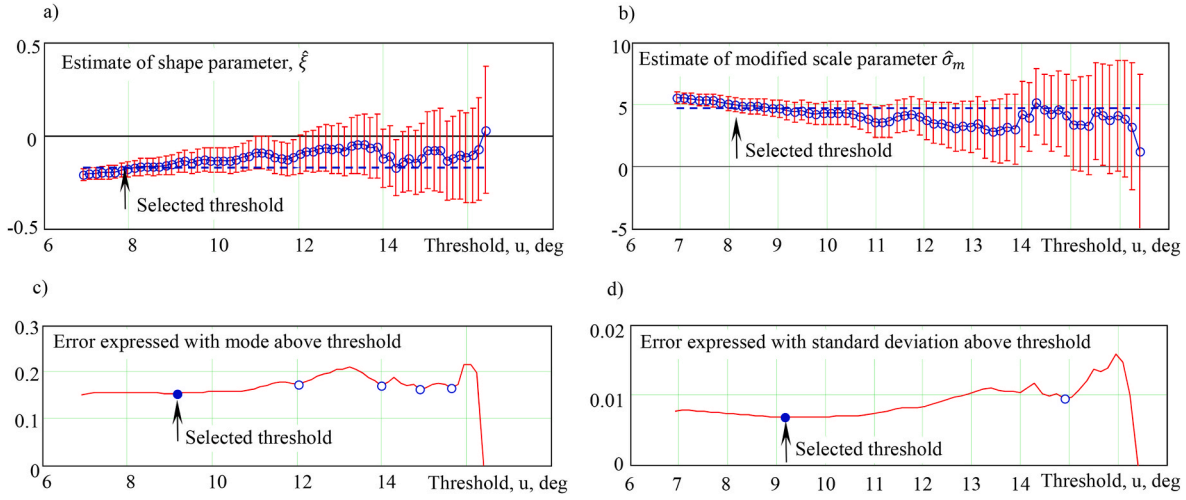

Fig. 6. Selection of threshold for GPD for data set 3 (a) stabilization of shape parameter estimate (b) stabilization of modified scale parameter (c) minimization of error expressed with mode above threshold (d) minimization of error expressed with standard deviation above threshold.

for the shape parameter to be positive or negative? Belenky et al. (2019) argues that the shape parameter has to be positive for the peaks of roll motion. The main points of the argument are reviewed below.

A single degree-of-freedom (1-DOF) dynamical system with a piecewise linear (PWL) restoring function is a convenient model for theoretical study. It provides a qualitatively correct topology of the phase plane and offers closed-form solutions for many interesting problems (Belenky, 2000). Consider the differential equation:

$$\ddot{\phi} + 2\delta\dot{\phi} + \omega_0^2 f_{PWL}(\phi) = f_{E\varphi}(t) \tag{10}$$

where δ is a linear damping coefficient and $f_{E\varphi}$ is a stationary stochastic process of roll excitation, while the roll restoring f_{PWL} is shown in Fig. 7.

$$f_{PWL}(\phi) = \begin{cases} k_2(\phi + \phi_{m1}) + k_1(\phi - \phi_{m0}) - \phi_{m0} & \text{if } \phi < -\phi_{m1} \\ -k_1(\phi + \phi_{m0}) - \phi_{m0} & \text{if } -\phi_{m1} \le \phi < -\phi_{m0} \\ \phi & \text{if } -\phi_{m0} \le \phi \le \phi_{m0} \\ -k_1(\phi - \phi_{m0}) + \phi_{m0} & \text{if } \phi_{m0} < \phi \le \phi_{m1} \\ k_2(\phi - \phi_{m1}) - k_1(\phi - \phi_{m0}) + \phi_{m0} & \text{if } \phi_{m1} < \phi \end{cases} \tag{11}$$

The slope coefficients for the piecewise linear terms k_1 and k_2 are defined as:

$$k_1 > 0\,; \quad k_2 = \frac{k_1(\phi_{m1} - \phi_{m0}) - \phi_{m0}}{\pi - \phi_{m1}}. \tag{12}$$

The differential equation (10) has a closed form solution within each range. As the equation (10) is linear within each range, the solution is presented as a sum of a general solution of the autonomous equation and a particular solution of heteronomous equation:

$$\phi = \begin{cases} \phi_a e^{-\delta t}\sin(\omega_{d0}t + \varepsilon) + p_0(t); & \text{if } -\phi_{m0} \le \phi \le \phi_{m0} \\ Ae^{\lambda_1 t} + Be^{\lambda_2 t} + p_1(t) + \phi_V; & \text{if } \phi_{m0} < \phi \le \phi_{m1} \\ \phi_{a2} e^{-\delta t}\sin(\omega_{d2}t + \varepsilon_2) + p_2(t) + \pi; & \text{if } \phi > \phi_{m1} \end{cases} \tag{13}$$

where ϕ_a, ε, A, B, ϕ_{a2} and ε_2 are arbitrary constants that are dependent on the initial conditions at the "switching" of the ranges; ω_{d0} and ω_{d2} are frequencies of the damped oscillation in ranges 0 and 2, respectively; λ_1 and λ_2 are eigenvalues for the solution in Range 1. p_0, p_1 and p_3 are particular solutions, similar in shape to the excitation $f_{E\varphi}$, i.e. stationary stochastic processes.

The system (10) has all the properties of a nonlinear system; Belenky (2000) describes its nonlinear properties, typical of the softening nonlinearity, including:

- Loss of isochronism, i.e. dependence of natural frequency on initial amplitude
- Fold bifurcation: coexistence of low- and high- amplitude stable response to mono-periodic excitation of the same frequency, observed for excitation frequencies slightly lower than the natural frequency
- Flip bifurcation: response period doubling sequence, leading to deterministic chaos under mono-periodic excitation with frequencies slightly higher than the natural frequency
- Erosion of the safe basin (set of initial conditions in the phase plane that do not lead to capsizing) for large-amplitude mono-periodic excitation, with the frequency close to the natural frequency

These phenomena are considered essential nonlinear behaviors, observed for a nonlinear dynamical system with softening nonlinearity – e.g. Duffing equation (Belenky and Sevastianov 2007). Equation (10) can, therefore, be considered a qualitative representation of a nonlinear dynamical system with softening nonlinearity. The latter is also considered as the simplest qualitative mathematical model of nonlinear roll motions.

As the dynamical system (10) may be seen as a qualitative mathematical model of nonlinear roll motions, consider a distribution of the local maxima of the solution (13) that exceeds the level of φ_{m0} but is not of capsizing.

A resonance phenomenon is not possible in Range 1 as the general solution of autonomous equation does not contain any oscillatory function. As a result:

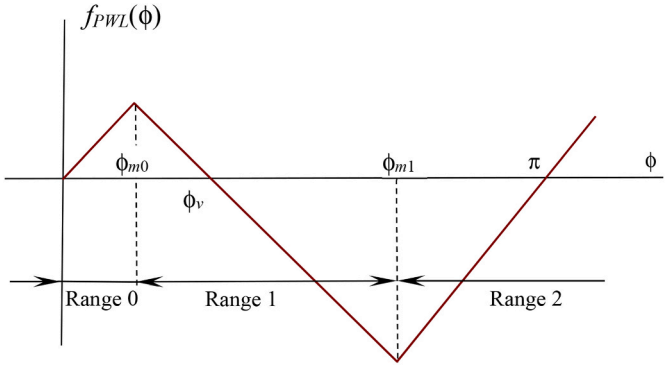

Fig. 7. Piecewise linear restoring term.

$$\mathrm{Var}(p_0) \gg \mathrm{Var}(p_1) \ll \mathrm{Var}(p_2), \tag{14}$$

where Var(..) is a variance operator. More details on this argument can be found in Belenky et al. (2023). The eigenvalues for the solution in the Range 2 are:

$$\lambda_{1,2} = -\delta \pm \sqrt{k_{f1}\omega_0^2 + \delta^2}, \tag{15}$$

where k_{f1} is the absolute value of the slope of the stiffness function in Range 1. For the sake of simplicity of further derivation, the damping is assumed to be absent in Range 1, so:

$$\lambda_1 = -\lambda_2 = \sqrt{k_{f1}\omega_0^2} = \omega_{d1}. \tag{16}$$

The solution (13) in Range 1 can then be expressed as:

$$\phi(t) = H\cosh(\omega_{d1}t + \varepsilon) + \phi_V \quad \text{if} \quad \phi_{m0} < \phi \le \phi_{m1}. \tag{17}$$

Arbitrary constants are expressed as:

$$H(\dot{\phi}_U) = -\frac{1}{\omega_{d1}}\sqrt{\omega_{d1}^2(\phi_{m0} - \phi_V)^2 - \dot{\phi}_U^2}, \tag{18}$$

$$\varepsilon(\dot{\phi}_U) = \tanh^{-1}\left(\frac{\dot{\phi}_U}{\omega_{d1}(\phi_{m0} - \phi_V)}\right). \tag{19}$$

where $\dot{\phi}_U$ is the roll rate at upcrossing. The value of the peak is expressed as

$$\phi_{\max}(\dot{\phi}_U) = H(\dot{\phi}_U) + \phi_V \;;\; 0 < \dot{\phi}_U \le \dot{\phi}_{Cr}, \tag{20}$$

where $\dot{\phi}_{Cr}$ is critical roll rate corresponding to capsizing conditions (Belenky et al., 2023 and the next section).

Within the accepted assumptions, all the quantities in (20) are constant with the exception of the roll rate at upcrossing $\dot{\phi}_U$. This is a random variable, as stochastic excitation has been kept for Range 0. Assuming that upcrossings are rare, the general solution of the autonomous equation in Range 0 will have enough time to subside between upcrossings, so the distribution of the roll rate at upcrossing follows Rayleigh (Leadbetter et al., 1983, p. 201). The distribution needs to be normalized for the condition of the absence of capsizing (if capsizing happens, the ship is not returning to its initial equilibrium, and no roll peak will occur):

$$\mathrm{PDF}(\dot{\phi}_U) = \left(1 - \exp\left(-\frac{\dot{\phi}_{Cr}^2}{2V_{\dot{\phi}}}\right)\right)\frac{\dot{\phi}_U}{V_{\dot{\phi}}}\exp\left(-\frac{\dot{\phi}_U^2}{2V_{\dot{\phi}}}\right), \quad 0 < \dot{\phi}_U \le \dot{\phi}_{Cr}, \tag{21}$$

where $V_{\dot{\phi}}$ is variance of roll rates.

The distribution (21) can be used even if the upcrossings are clustered, see Belenky et al. (2019) for details. Equation (20) is a deterministic function of a single random variable with known distribution and the function is monotonic, so the distribution of the roll peaks/local maxima of the roll angles can be found and expressed as:

$$\mathrm{PDF}(\phi_{\max}) = pdf\left(G^{-1}(\phi_{\max})\right)\left|\frac{dG^{-1}(\phi_{\max})}{d\phi_{\max}}\right|, \quad 0 < \phi_{\max} \le \phi_V. \tag{22}$$

G^{-1} is an inverse of the function defined in equation (20):

$$G^{-1}(\phi_{\max}) = \omega_{d1}\sqrt{(\phi_{m0} - \phi_V)^2 - (\phi_{\max} - \phi_V)^2}. \tag{23}$$

As a result, the distribution density of the roll peaks is expressed in the following form:

$$\mathrm{PDF}(\phi_{\max}) = \frac{\phi_V - \phi_{max}}{C}\exp\left(-\frac{\omega_{d1}^2(\phi_{m0} - \phi_V)^2}{2V_{\dot{\phi}}}\right), \quad 0 < \phi_{\max} \le \phi_V, \tag{24}$$

where

$$C = \frac{V_{\dot{\phi}}}{\omega_{d1}^2}\left(\exp\left(-\frac{\omega_{d1}^2(\phi_{m0} - \phi_V)^2}{2V_{\dot{\phi}}}\right) - 1\right). \tag{25}$$

As equation (24) presents the entire distribution of roll peaks for the piecewise linear system, it contains insight into how the PWL response differs from the linear response. The distribution of the peaks of a linear response can be approximated by a truncated Rayleigh distribution (*e.g.* Belenky and Campbell, 2012):

$$\mathrm{PDF}(\phi_{max}) = C_L\frac{\phi_{max}}{V_\phi}\exp\left(-\frac{\phi_{max}^2}{2V_\phi}\right), \quad \phi_{max} > \phi_{m0}, \tag{26}$$

where V_ϕ is the variance of roll and C_L is a normalizing constant:

$$C_L = \exp\left(-\frac{\phi_{m0}^2}{2V_\phi}\right). \tag{27}$$

Fig. 8 has both PDFs. The peaks of the linear response are expected to follow an exponential tail, so the PWL response peaks have a heavy tail. The tail remains heavy until a large value near the angle of vanishing stability. The tail then becomes light, creating an inflection point. This inflection point is caused by the non-capsizing condition: closer to the angle of vanishing stability means more trajectories lead to capsizing. As the inflection point is close to the angle of vanishing stability, the tail of PWL peaks is heavy for most of Range 1 as is expected.

Belenky et al. (2019) describes a solution without assuming zero damping in Range 1. The complete PDF cannot be expressed as a closed-form function but its behavior at the limit, when the roll angle approaches the angle of vanishing stability, points to a heavy tail.

A completely different approach described in Belenky et al. (2019) assumes that the excitation is white noise and obtains the PDF from the Fokker-Plank-Kolmogorov (FPK) equation. While a realistic excitation is, of course, far from white noise, the shape of the PDF of a nonlinear response seems to be the same for weakly correlated or uncorrelated excitation (Maki, 2017). For the qualitative study described in this section, the assumption of white noise excitation seems to be quite appropriate.

The FPK approach not only confirms that the tail is heavy but explains why. It is a result of the stretching of the phase plane caused by softening nonlinearity, as illustrated in Fig. 9a. The PDF in Fig. 9b indicates three different types of behavior: Gaussian, corresponding to the Range 0 (area I), heavy tail (area II) and light tail in the Range 1 (area III) caused by the increased number of capsizings.

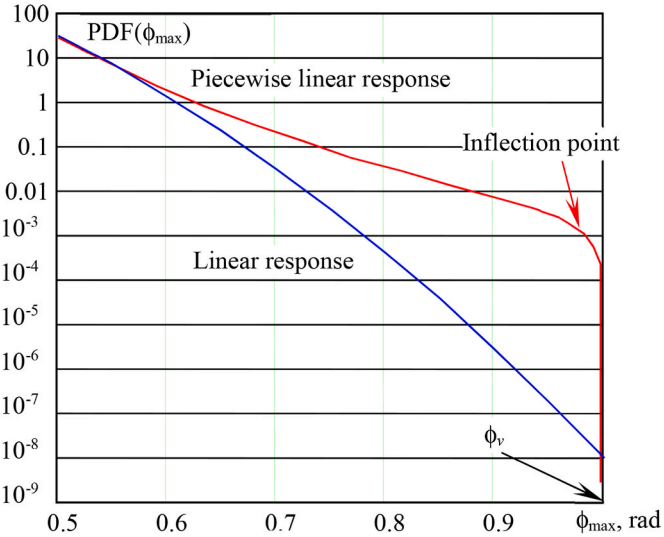

Fig. 8. PDFs of peaks of linear response and piecewise response.

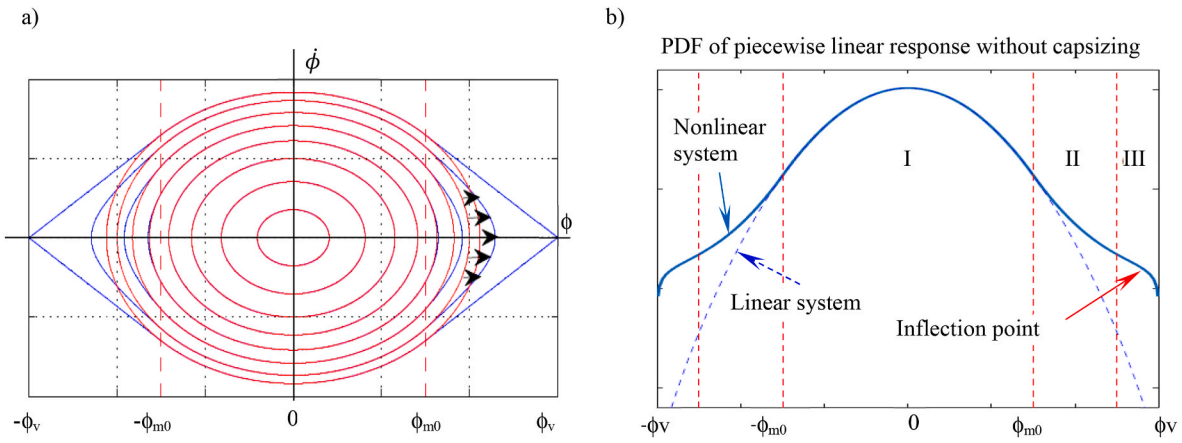

Fig. 9. (a) Phase plane for the linear and PWL system (b) PDF for both systems.

Another way to illustrate this stretching is to compare short portions of the time histories of the piecewise linear and linear systems, starting with some positive roll rate from the angle φ_{m0} in Fig. 10. The response of the linear system is described by a trigonometric function, sine or cosine, with appropriate phase shift. The PWL response in the absence of capsizing is described by a hyperbolic cosine, equation (17). Hyperbolic cosine always stays above the trigonometric cosine for the same initial conditions.

The PWL system spends more time in Range 1 than the linear system under the same initial conditions. As a result, the probability of finding the PWL system in Range 1 is higher and the tail of the response is heavier than the linear example. As both responses start from the same initial roll rate, the maximum of the PWL response must be larger than the linear case. Thus, the tail of peaks of the PWL response is heavier than the linear case in Fig. 8.

5. Behavior of distribution tail of the roll peaks

To test the theoretical conclusion of a heavy tail for the roll peak, the estimation of shape parameter was performed on the larger volume of the 3-DOF SimpleCode data for the tumblehome hull at eight different heading angles, shown in Table 3. These data sets have a ship speed of 6 knots and wave parameters of 9 m significant wave height and 15 s

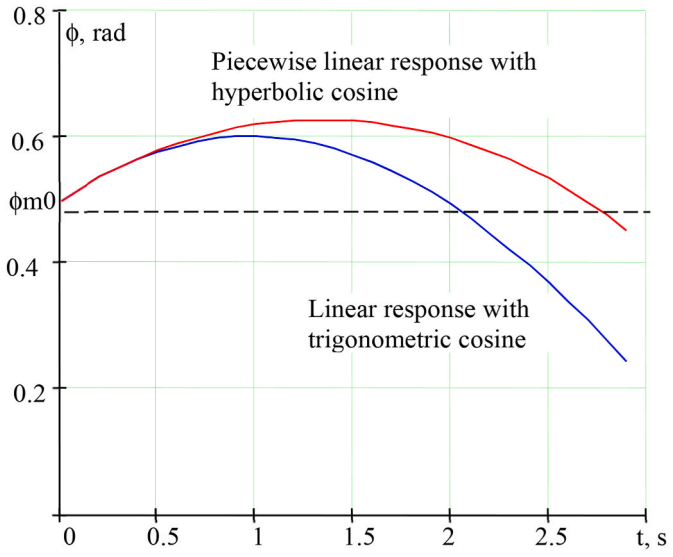

Fig. 10. Piecewise linear response above the knuckle point vs. linear response (Belenky et al., 2019).

Table 3
Conditions for study of shape parameter.

Heading deg.	Time, hrs.	Heading deg.	Time, hrs.
15	10,000	45	10,000
22.5	10,000	60	13,500
30	10,000	90	10,000
37.5	10,000	135	7,000

modal period as described in Section 2. These data was used to estimate the shape parameter for a series of thresholds and construct the confidence intervals as described in Campbell et al. (2016) or Belenky et al. (2023). The results are shown in Fig. 11.

As the probability of the exceedance of a large roll angle significantly depends on the heading angle, the range of the thresholds for each heading angle is quite different in Fig. 11. The longest range has been observed for 60° heading, which also has the largest volume of sample. The different lengths of these ranges makes comparison of the shape parameter behavior more difficult, as shorter ranges do not necessarily demonstrate the complete picture.

The change of the heading angles is expected to change the contribution of stability variation and excitation in the likelihood of large roll angles. At the smallest (closest to following seas) heading angles of 15° and 22.5°, the variation of stability is expected to be the largest, but the wave excitation of roll would be relatively small. In long-crested waves, the wave excitation is zero in exactly following seas. At 45° and 60° heading, the roll angles are the largest as stability variation is still strong, while the wave excitation is already strong. At 90°, the range of thresholds decreases as the contribution from stability variation disappears. As far as the 135° heading is concerned, the stability variation is present there, but cannot significantly influence the dynamics of roll as the encounter frequency becomes larger.

The time interval of decreased stability still exists, but is too short for the ship to react with a large roll angle. That is why the headings 15–60° are considered separately, as the stability variation in waves is a significant factor. Based on this argument, the structure of the tail of the roll peaks can be hypothesized to be the same across this heading range and the difference between Fig. 11a through 11f is a result of not observing all of the present phenomena for the smaller heading angles.

The shape parameter in Fig. 11g is estimated from the beam seas data, where stability variation is not expected. The data exhibits bimodality: the estimate becomes positive around 15°, than drops to zero at around 20° and has a tendency to increase after 24°. The latter tendency is an estimate, as the confidence interval becomes wide due to small sample volume at large thresholds. The 1-DOF reduced-order model (ROM) shows a combination of heavy and light tails.

The appearance of a light tail in the ROM was explained by capsizing,

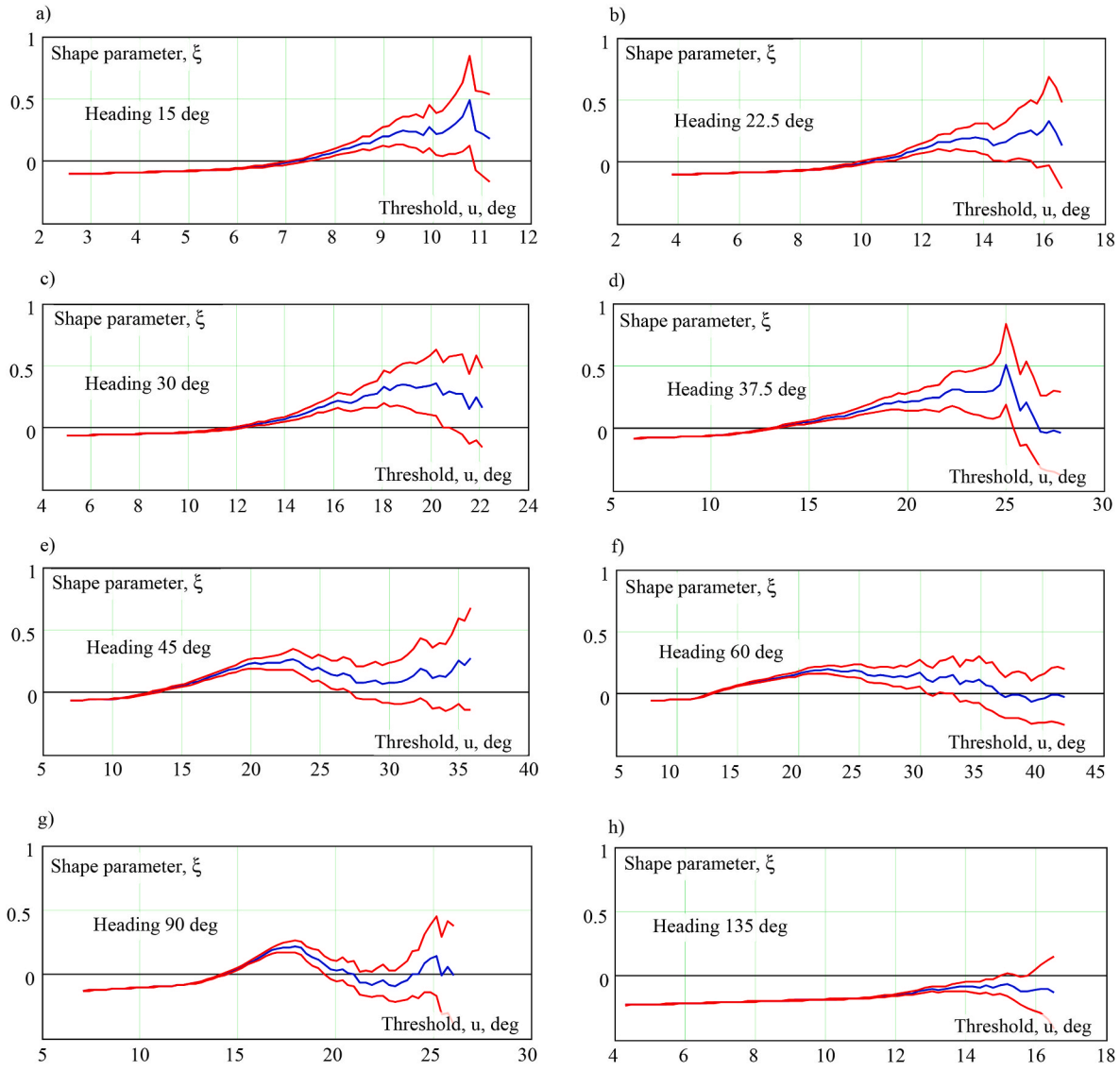

Fig. 11. Behavior of shape parameter estimated over a large volume of data: blue line is a mean value of shape parameter, red lines are boundaries of confidence interval; (a) heading 15 deg. (b) heading 22.5 deg. (c) heading 30 deg. (d) heading 37.5 deg. (e) heading 45 deg. (f) heading 60 deg. (g) heading 90 deg. (h) heading 135 deg.

eliminating the population of roll peaks (a peak event is mutually exclusive with a capsizing event), but this was occurring close to the angle of vanishing stability. A plausible hypothesis is an energy transfer to another degree of freedom. As a result of this energy transfer, the population of large roll peaks can be decreased, leading to a decrease of the estimate of shape parameter.

The energy transfer to other degrees of freedom may also be responsible for decreasing of the shape parameter estimates observed for 45° and 60° of heading respectively (Fig. 11e and 11f). It seems to be occurring for larger thresholds: the first peak of the shape parameter estimate is around 18° for beams seas, while it shifts to about 22° for the headings of 45 and 60°. Stability variation is an apparent explanation for this shift.

The estimate of shape parameter for 135° heading (bow seas) seems to stabilize around the threshold of 14° with a negative value. Being the smallest sample in the shape parameter study, this case probably needs significantly more data for a conclusion. The wave excitation in oblique seas is reduced by heading and a widening of encounter spectrum (less energy in the resonance range), while stability variation does not affect the dynamics as much.

If the hypothesis of energy transfer to other degrees of freedom is correct, energy transfer needs to be modeled with a ROM. However, at this time, it is considered a second-order influence, compared to the nonlinearity of the GZ curve. The assumption of heavy tail still stands for the first expansion, keeping in mind, that it is supported by the statistical validation by Campbell et al. (2023).

6. Fitting the heavy tail

6.1. Power law or Pareto tail

To approximate a heavy tail of roll peaks, consider the GPD for $\xi > 0$ and set $u = \sigma/\xi$:

$$\begin{aligned}\mathrm{PDF}_{GPD}(x) &= \frac{1}{\sigma}\left(1+\xi\frac{x-u}{\sigma}\right)^{-(1+1/\xi)} = \frac{1}{\sigma}\left(1+\xi\frac{x-\sigma/\xi}{\sigma}\right)^{-(1+1/\xi)} \\ &= \frac{1}{\sigma}\left(\frac{\sigma/\xi}{x}\right)^{1+1/\xi} = \frac{1}{\sigma}\frac{(\sigma/\xi)^{1+1/\xi}}{x^{1+1/\xi}} = \frac{1}{\xi}\frac{(\sigma/\xi)^{1/\xi}}{x^{1+1/\xi}}.\end{aligned} \tag{28}$$

Using $x_m = \sigma/\xi = u$ and $\alpha = 1/\xi$, equation (28) is known as Pareto distribution:

$$\mathrm{PDF}_P(x) = \alpha \frac{x_m^\alpha}{x^{1+\alpha}}, x \geq x_m, \alpha > 0. \tag{29}$$

The CDF is expressed as:

$$\mathrm{CDF}_P(x) = \int_{x_m}^{x} \alpha \frac{x_m^\alpha}{y^{1+\alpha}} dy = 1 - \left(\frac{x_m}{x}\right)^\alpha, x \geq x_m; \alpha > 0, \tag{30}$$

leading to the following equation for the distribution tail:

$$P(X > x) = \left(\frac{x_m}{x}\right)^\alpha, x \geq x_m, \alpha > 0. \tag{31}$$

In general, the Pareto distribution can be used to approximate a heavy tail of any distribution. This type of tail is also referred as a "power law" tail to reflect the structure of equation (31). A distribution of a positive variable is said to have a power-law Pareto tail if

$$P(X > x) = C(x)x^{-\alpha}, \ x > 0, \ \alpha > 0. \tag{32}$$

$C(x)$ is the so-called "slowly varying" function at infinity. The simplest example of such a slowly varying function is any positive function satisfying $C(x) \sim C$ with a positive constant C as x approaches infinity. Another example would be for $C(x) \sim x$ as x increases. Following the results from the previous section, the distribution of the envelope of the peaks of roll motion is suggested to be heavy-tailed.

The Pareto distribution has an important property: it becomes exponential if its argument is

$$w = G(x) = \ln(x) - \ln(x_m). \tag{33}$$

To find a distribution of a function of a random variable $G(x)$, one needs to invert this function and differentiate the inverse function (see section 5.7 of Ross (1997) or chapter 7 of Walpole et al. (2012)):

$$G^{-1}(w) = x_m \exp(w); \quad \frac{dG^{-1}(w)}{dw} = x_m \exp(w). \tag{34}$$

The distribution of $w = G(x)$ is then expressed as:

$$\mathrm{PDF}(w) = \mathrm{PDF}_P\left(G^{-1}(w)\right) \frac{dG^{-1}(w)}{dw} = \frac{\alpha x_m^\alpha x_m \exp(w)}{(x_m \exp(w))^{1+\alpha}} = \alpha \exp(-\alpha w). \tag{35}$$

The PDF (35) is an exponential distribution with parameter α. Recall that the mean value and variance of an exponential random variable are expressed as:

$$\mathbb{E}(\mathrm{w}) = \frac{1}{\alpha} = \xi; \quad \mathrm{Var}(\mathrm{w}) = \frac{1}{\alpha^2} = \xi^2. \tag{36}$$

The Pareto distribution has only one parameter – the shape parameter – to fit. The value x_m plays the role of the threshold and it is selected to minimize the fitting error. So the shape parameter needs to be estimated first. While the shape parameter is essentially the same as for the GPD, it make sense to use a different symbol as the methods for estimating the parameters are different for GPD and the power law/Pareto tail:

$$\gamma = \frac{1}{\alpha} = \xi. \tag{37}$$

As the estimation of the parameter γ needs to be done for a series of candidate thresholds (as was done for the GPD case), it is convenient to sort the data in descending order:

$$\overrightarrow{\varphi} = \mathrm{sort}_{\mathrm{desc}}\left(\overrightarrow{\phi}_{ep}\right) \Rightarrow \varphi_n \leq \ldots \leq \varphi_1, \tag{38}$$

$\overrightarrow{\phi}_{ep}$ are the mean-crossing peaks of the envelope of roll motions (see Fig. 3b). The vector $\overrightarrow{\varphi}$ is the upper order statistics of the data – i.e. the observed values, sorted in descending order.

A number of ways to estimate the parameter γ have been proposed in the literature (e.g. Beirlant et al., 2004). The most commonly used estimator of γ is the Hill estimator defined as

$$\widehat{\gamma}_k = \frac{1}{k} \sum_{j=1}^{k} \left(\ln(\varphi_j) - \ln(\varphi_{k+1})\right). \tag{39}$$

The index k refers to the number of upper order statistics used in the estimation, so the index $k+1$ refers to the index corresponding to the candidate threshold, *i.e.* $\varphi_{k+1} = u$:

$$\begin{aligned} \varphi_n \leq \varphi_{n-1} \leq \ldots \leq \varphi_{k+2} \leq (\varphi_{k+1} = u) \\ \leq \underbrace{\varphi_k \leq \varphi_{k-1} \leq \ldots \leq \varphi_2 \leq \varphi_1}_{k}. \end{aligned} \tag{40}$$

Note that the Hill estimator is essentially an average of the logarithm of data values above the threshold. As the logarithm of the data values (33) follows exponential distribution (35), the Hill estimator (39) is consistent with equation (36). For a large k,

$$\sqrt{k}(\widehat{\gamma}_k - \gamma) \approx \mathcal{N}(0, \gamma^2). \tag{41}$$

$\mathcal{N}(\mu, V)$ refers to a normal distribution with mean μ and variance V, which can be used to set confidence intervals in the standard way.

6.2. Finding a threshold for power law/Pareto tail model

A number of methods are also available to select the index k or threshold $u = \varphi_{k+1}$, above which the distribution is considered to be power-law or Pareto in the form:

$$P(\varphi > \varphi^*) = \left(\frac{u}{\varphi^*}\right)^{1/\gamma}, \ \varphi^* > u. \tag{42}$$

One of these methods is based on the so-called prediction error criterion (Dupuis and Victoria-Feser, 2006; Mager, 2015). Let

$$s_i = \ln(\varphi_i) - \ln(u), \ i = 1, \ldots, k. \tag{43}$$

The prediction criterion concerns the mean squared prediction error, defined as (using symbol $\mathbb{E}$ for averaging):

$$\Gamma(k) = \frac{1}{k} \sum_{i=1}^{k} \mathbb{E}\left(\frac{\widehat{s}_i - \mathbb{E}(s_i)}{\sqrt{V_i}}\right)^2, \tag{44}$$

where $V_i = \mathrm{Var}(s_i)$ is the variance and $\widehat{s}_i$ is the estimated value of s_i according to the model with power-law Pareto tail of distribution. Following Lemma 4.2 in Mager (2015), one can consider expected value of square of the difference between random variable a andthe expected value of a random variable b, where a and b are correlated, *i.e.* $\mathrm{Cov}(a, b) \neq 0$:

$$\begin{aligned} \mathbb{E}\left((a - \mathbb{E}(b))^2\right) &= \mathbb{E}\left(a^2 - 2a\mathbb{E}(b) + (\mathbb{E}(b))^2\right) \\ &= \mathbb{E}\left(a^2\right) - 2\mathbb{E}(a)\mathbb{E}(b) + (\mathbb{E}(b))^2 \\ &= \mathbb{E}\left(a^2\right) - 2\mathbb{E}(a)\mathbb{E}(b) + (\mathbb{E}(b))^2 \\ &\quad + 2\mathbb{E}(ab) - 2\mathbb{E}(ab) + \mathbb{E}\left(b^2\right) - \mathbb{E}\left(b^2\right) \\ &= \underbrace{\mathbb{E}\left(a^2\right) - 2\mathbb{E}(ab) + \mathrm{E}\left(b^2\right)}_{\mathbb{E}\left((a-b)^2\right)} + \underbrace{2\mathbb{E}(ab) - 2\mathbb{E}(a)\mathbb{E}(b)}_{2\mathrm{Cov}(a,b)} \\ &\quad - \underbrace{\left(\mathbb{E}\left(b^2\right) - (\mathbb{E}(b))^2\right)}_{\mathrm{Var}(b)} \\ &= \mathbb{E}\left((a - \mathrm{b})^2\right) + 2\mathrm{Cov}(a, b) - \mathrm{Var}(b). \end{aligned} \tag{45}$$

Substituting (45) into (44), the mean squared prediction error $\Gamma(k)$ can be expressed as:

$$\Gamma(k) = \frac{1}{k} \sum_{i=1}^{k} \mathbb{E}\left(\frac{\widehat{s}_i - s_i}{\sqrt{V_i}}\right)^2 + \frac{2}{k} \sum_{i=1}^{k} \frac{\mathrm{Cov}(\widehat{s}_i, s_i)}{V_i} - 1. \tag{46}$$

As the variance of the data above the threshold $V_i = \mathrm{Var}(s_i)$ is not known, it is substituted by its estimate $\widehat{V}_i = \widehat{\mathrm{Var}}(s_i)$. The covariance $\mathrm{Cov}(\widehat{s}_i, s_i)$ is also substituted by its estimate $\widehat{\mathrm{Cov}}(\widehat{s}_i, s_i)$. Note that the symbol "hat" is used here with two slightly different meanings: $\widehat{s}_i$ is a

value estimated by power-law Pareto tail model (31), while s_i are observed values above the threshold u, equation (43). Quantities $\widehat{V}_i$ and $\widehat{\mathrm{Cov}}(\widehat{s}_i, s_i)$ are estimated from these observed values, leading to the estimated prediction error:

$$\widehat{\Gamma}(k) = \frac{1}{k}\sum_{i=1}^{k}\left(\frac{\widehat{s}_i - s_i}{\sqrt{\widehat{V}_i}}\right)^2 + \frac{2}{k}\sum_{i=1}^{k}\frac{\widehat{\mathrm{Cov}}(\widehat{s}_i, s_i)}{\widehat{V}_i} - 1. \tag{47}$$

The index for the selected threshold u is chosen as that minimizing $\widehat{\Gamma}(k)$ over some range of values k. Mager (2015) suggests setting the range $[\max(40, 0.02n), 0.2n]$.

To conclude the description of the method, the quantities of $\widehat{s}_i$, $\widehat{\mathrm{Var}}(s_i)$ and $\widehat{\mathrm{Cov}}(\widehat{s}_i, s_i)$ in the definition of $\widehat{\Gamma}(k)$ need to be specified.

6.3. Order statistics and their variance

Further considerations require application of the apparatus of order statistics (*e.g.* David and Nagaraja, 2005), which is widely used in financial applications but relatively rare in engineering. Note that order statistics are defined in ascending order, while here the sorting is done in descending order (see equation (38)). The term "upper order statistics" indicates sorting in descending order. A distribution of k-th order statistics for a sample with n points is expressed as:

$$\mathrm{PDF}_k(x) = \frac{n!}{(k-1)!(n-k)!}\mathrm{PDF}(x)(\mathrm{CDF}(x))^{k-1}(1-\mathrm{CDF}(x))^{n-k}. \tag{48}$$

For upper order statistics, the distribution is (Embrechts et al., 2013, Proposition 4.1.2)

$$\mathrm{PDF}_k(x) = \frac{n!}{(k-1)!(n-k)!}\mathrm{PDF}(x)(1-\mathrm{CDF}(x))^{k-1}(\mathrm{CDF}(x))^{n-k}. \tag{49}$$

The cited reference also contains a formula and a heuristic argument (as the data points are independent and there are $n!$ ways to collect n numbers) for the joint distribution of all n upper order statistics:

$$\mathrm{PDF}(x_1, \ldots, x_n) = n!\prod_{i=1}^{n}\mathrm{PDF}(x_i), \quad x_1 > x_2 > \ldots > x_n. \tag{50}$$

As shown in equations 34 and 35, the logarithm function (33) of Pareto-distributed argument follows exponential distribution with mean γ. Consider joint distribution of upper order statistics y of independent variables following exponential distribution with mean $\gamma = 1$:

$$\begin{aligned}&\mathrm{PDF}_{E1}(y_1, \ldots, y_n) = n!\exp\left(-\textstyle\sum_{i=1}^{n} y_i\right),\\ &\quad y_1 > y_2 > \ldots > y_n.\end{aligned} \tag{51}$$

Consider joint distribution of scaled differences between the upper order statistics, referred to as "spacing" in Example 4.1.5 from Embrechts et al. (2013), and defined as:

$$\begin{aligned}&\vec{z}^{\,T} = (y_1 - y_2, 2(y_2 - y_3), \ldots, (n-1)(y_{n-1} - y_n), n y_n)\\ &\text{or} \quad z_i = i(y_i - y_{i+1});\ i = 1, \ldots n+1 \text{ with } \quad y_{n+1} = 0,\end{aligned} \tag{52}$$

where superscript T indicates transposition. While $y_1 > y_2 > \ldots > y_n$, note $z_i > 0$, $i = 1, \ldots, n$. Transformation from the vector $\vec{y} = (y_1, \ldots, y_n)^T$ to $\vec{z}$ is defined as:

$$\vec{z} = \mathrm{H}(\vec{y}) = \mathbf{M}\,\vec{y}, \tag{53}$$

$$\mathbf{M} = \begin{pmatrix} 1 & -1 & 0 & \ldots & 0 \\ 0 & 2 & -2 & \ldots & 0 \\ 0 & 0 & 3 & \ldots & 0 \\ \ldots & \ldots & \ldots & \ldots & \ldots \\ 0 & 0 & 0 & \ldots & n \end{pmatrix}. \tag{54}$$

The distribution of the spacing is expressed as (e.g. chapter 6.7 of Ross, 1997):

$$\mathrm{PDF}(\vec{z}) = \mathrm{PDF}_{E1}\left(\mathrm{H}^{-1}(\vec{z})\right)\ \left|\det\left(\mathbf{J}\left(\mathrm{H}^{-1}(\vec{z})\right)\right)\right|, \tag{55}$$

where $\mathrm{H}^{-1}(\vec{z})$ is the inverse of transformation (53) and $\mathbf{J}$ is its Jacobian matrix:

$$\vec{y} = \mathrm{H}^{-1}(\vec{z}) = \vec{z}^{\,T}\,\mathbf{M}^{-1}, \tag{56}$$

$$\mathbf{M}^{-1} = \begin{pmatrix} 1 & 2^{-1} & 3^{-1} & \ldots & n^{-1} \\ 0 & 2^{-1} & 3^{-1} & \ldots & n^{-1} \\ 0 & 0 & 3^{-1} & \ldots & n^{-1} \\ \ldots & \ldots & \ldots & \ldots & \ldots \\ 0 & 0 & 0 & \ldots & n^{-1} \end{pmatrix}. \tag{57}$$

As the inverse transformation (56) is linear, $\mathbf{J}(\mathrm{H}^{-1}(\vec{z})) = \mathbf{M}^{-1}$ and

$$\det\left(\mathbf{J}\left(\mathrm{H}^{-1}(\vec{z})\right)\right) = \det\left(\mathbf{M}^{-1}\right) = (\det(\mathbf{M}))^{-1} = (n!)^{-1}. \tag{58}$$

The inverse transformation (56) can be expressed as a vector:

$$\begin{aligned}&\vec{y} = \left(\textstyle\sum_{j=1}^{n}\frac{z_j}{j}, \sum_{j=2}^{n}\frac{z_j}{j}, \ldots, \frac{z_n}{n}\right)^T, \quad \text{or}\\ &\quad y_i = \textstyle\sum_{j=i}^{n}\frac{z_j}{j};\ \ i = 1, \ldots n.\end{aligned} \tag{59}$$

Substitution of equations (51), (58) and (59) into equation (55) leads to the following distribution for $\vec{z}$:

$$\mathrm{PDF}_z(z_1, \ldots, z_n) = \exp\left(-\sum_{i=1}^{n}\sum_{j=i}^{n}\frac{z_j}{j}\right) = \exp\left(-\sum_{i=1}^{n} z_j\right) \tag{60}$$

as

$$\begin{aligned}\sum_{i=1}^{n}\sum_{j=i}^{n}\frac{z_j}{j} = {} & z_1 + \frac{z_2}{2} + \frac{z_3}{3} + \ldots + \frac{z_n}{n} + \frac{z_2}{2} + \frac{z_3}{3} + \ldots + \frac{z_n}{n} + \frac{z_3}{3} + \ldots + \frac{z_n}{n}\\ & \ldots\\ & + \frac{z_n}{n}\\ = {} & \sum_{i=1}^{n} z_i.\end{aligned}$$

The equation (60) is the distribution of n independent exponential random variables with parameter 1. The variance of each of the component of vector $\vec{z}$ is unity, i.e. $\mathrm{Var}(z_i) = 1$. Recalling that the underlying random variables of upper order statistics s_i, defined in equation (43), follow exponential distribution with mean γ, then:

$$s_i = \gamma y_i = \gamma\sum_{j=i}^{k}\frac{z_j}{j}. \tag{61}$$

The variance of the i-th upper order statistic is:

$$V_i = \mathrm{Var}(s_i) = \gamma^2\sum_{j=i}^{k}\frac{\mathrm{Var}(z_i)}{j^2} = \gamma^2\sum_{j=i}^{k}\frac{1}{j^2}, \tag{62}$$

which can be estimated as:

$$\widehat{V}_i = \widehat{\gamma}_k^2\sum_{j=i}^{k}\frac{1}{j^2}, \tag{63}$$

where $\widehat{\gamma}_k$ is defined with equation (39).

6.4. Covariance of the order statistics and estimates at the tail

The estimator $\widehat{s}_i$ of s_i is defined as follows. The quantity s_i can be thought as the $(1 - i/(k+1))^{th}$ quantile of the exponential distribution:

$$\frac{i}{k+1} = \exp\left(-\frac{\widehat{s}_i}{\widehat{\gamma}_k}\right) \Longleftrightarrow \widehat{s}_i = -\widehat{\gamma}_k\ln\left(\frac{i}{k+1}\right). \tag{64}$$

To find the covariance $\mathrm{Cov}(\widehat{s}_i, s_i)$ for equation (46), equations (43) and (39) can substituted into (64), yielding the following expression for the estimated value in the tail $\widehat{s}_i$:

$$\widehat{s}_i = -\ln\left(\frac{i}{k+1}\right)\frac{1}{k}\sum_{j=1}^{k} s_j. \tag{65}$$

The formula (65) is used in $\mathrm{Cov}(\widehat{s}_i, s_i)$, recalling that k is the index for the candidate threshold $u = s_{k+1}$ and i is a counter in a sum in the prediction error $\Gamma(k)$, defined by equation (46). So, for a particular candidate threshold index k and the i-th term in (46), the term $\ln(1 - i/(k+1))$ is a constant. Also, the operations of summation and computation of covariance can be swapped:

$$\begin{aligned}\mathrm{Cov}(\widehat{s}_i, s_i) &= -\frac{1}{k}\ln\left(\frac{i}{k+1}\right)\mathrm{Cov}\left(\sum_{j=1}^{k} s_j, s_i\right)\\ &= -\frac{1}{k}\ln\left(\frac{i}{k+1}\right)\sum_{j=1}^{k}\mathrm{Cov}(s_j, s_i).\end{aligned} \tag{66}$$

The upper order statics s_i can be expressed through spacings z_i that are independent random variables following exponential distribution, see equation (61).

$$\mathrm{Cov}(s_j, s_i) = \mathrm{Cov}\left(\gamma\sum_{m=j}^{k}\frac{z_m}{m}, \gamma\sum_{j=i}^{k}\frac{z_j}{j}\right) = \gamma^2\sum_{m=j}^{k}\sum_{j=i}^{k}\frac{1}{mj}\mathrm{Cov}(z_m, z_j). \tag{67}$$

As the random variables z_i are exponentially distributed with mean 1, their variance is also 1. As they are also independent, the covariance is zero unless the indexes are the same.

$$\mathrm{Cov}(z_m, z_j) = \begin{cases} 1 & if\ j = m \\ 0 & \text{otherwise} \end{cases} \tag{68}$$

The double sum in equation (67) can be substituted with a single sum with the summation starting from the maximum of the indexes of i and j:

$$\mathrm{Cov}(s_j, s_i) = \gamma^2\sum_{m=\max(j,i)}^{k}\frac{1}{m^2} = \gamma^2\begin{cases}\sum_{m=i}^{k}\frac{1}{m^2} & \text{if} j \le i \\ \sum_{m=j}^{k}\frac{1}{m^2} & \text{otherwise}\end{cases} \tag{69}$$

Then, presenting sum in (67) in two components

$$\begin{aligned}&\sum_{j=1}^{k}\mathrm{Cov}(s_j, s_i)\\ &= \sum_{j=1}^{i}\mathrm{Cov}(s_j, s_i) + \sum_{j=i+1}^{k}\mathrm{Cov}(s_j, s_i)\\ &= \gamma^2\left(\sum_{j=1}^{i}\sum_{m=i}^{k}\frac{1}{m^2} + \sum_{j=i+1}^{k}\sum_{m=j}^{k}\frac{1}{m^2}\right)\\ &= \gamma^2\left(i\sum_{m=i}^{k}\frac{1}{m^2} + \sum_{j=i+1}^{k}\sum_{m=j}^{k}\frac{1}{m^2}\right).\end{aligned} \tag{70}$$

A sum of $1/m^2$ can be approximated as

$$\sum_{m=i}^{k}\frac{1}{m^2} \approx \int_i^{k+1}\frac{dx}{x^2} = \frac{k+1-i}{i(k+1)} \approx \frac{1}{k}\left(\frac{k+1}{i} - 1\right). \tag{71}$$

Using this approximation in (70) yields:

$$\sum_{j=1}^{k}\mathrm{Cov}(s_j, s_i) \approx \frac{\gamma^2}{k}\left(1 + \sum_{j=i+1}^{k}\frac{k+1}{j}\right). \tag{72}$$

Recognizing that for relatively large k

$$\begin{aligned}&\frac{1}{k}\left(1 + \sum_{j=i+1}^{k}\frac{k+1}{j}\right) \approx \sum_{j=i+1}^{k}\frac{1}{j}\\ &\approx \int_i^{k+1}\frac{dx}{x} = ln\left(\frac{k+1}{i}\right),\end{aligned} \tag{73}$$

and using (72) in (66), one can get

$$\mathrm{Cov}(\widehat{s}_i, s_i) \approx -\frac{\gamma^2}{k}\ln\left(\frac{k+1}{i}\right)\ln\left(\frac{i}{k+1}\right) = \frac{\gamma^2}{k}\left(\ln\left(\frac{i}{k+1}\right)\right)^2, \tag{74}$$

suggesting the use of:

$$\widehat{\mathrm{Cov}}(\widehat{s}_i, s_i) = \frac{\widehat{\gamma}_k^2}{k}\left(\ln\left(\frac{i}{k+1}\right)\right)^2. \tag{75}$$

6.5. Extrapolation estimate and its uncertainty

Substituting quantities from equations (63), (64) and (75) into the definition of $\widehat{\Gamma}(k)$ from equation (47) leads to a computable expression for the prediction error function:

$$\begin{aligned}\widehat{\Gamma}(k) = &\frac{1}{k\,\widehat{\gamma}_k^{\,2}}\sum_{i=1}^{k}\left(\sum_{j=i}^{k}\frac{1}{j^2}\right)^{-1}\left(s_i + \widehat{\gamma}_k\ln\left(\frac{i}{k+1}\right)\right)^2\\ &+\frac{2}{k^2}\sum_{i=1}^{k}\left(\sum_{j=i}^{k}\frac{1}{j^2}\right)^{-1}\left(\ln\left(\frac{i}{k+1}\right)\right)^2 - 1.\end{aligned} \tag{76}$$

The threshold u is selected as a minimum of the prediction error function $\widehat{\Gamma}(k)$.

$$k = \mathrm{argmin}(\widehat{\Gamma}(k)\,);\ u = \varphi_k. \tag{77}$$

Once the threshold has been selected, the Hill estimator $\widehat{\gamma}$ is computed with equation (39)

An example of $\widehat{\Gamma}(k)$, computed for data set 1, is shown in Fig. 12. The selected thresholds, number of points above these thresholds and resulting value of the Hill estimator (39) are presented in the Table 4. As it can be seen from Table 4, the values of the thresholds and Hill estimators are relatively close for all three data sets.

An estimate of the probability of exceedance of the target value, under the condition that the threshold u has been also exceeded, is competed with formula (31):

$$\widehat{P}(\phi > \phi^* | \varphi > u) = \left(\frac{\phi^*}{u}\right)^{-\frac{1}{\gamma}}. \tag{78}$$

To construct a confidence interval of the extrapolated estimate, the variance of the Hill estimator from equation (39) is expressed as follows (see equation (41)):

$$\widehat{V}_\gamma = \frac{\widehat{\gamma}^2}{k}. \tag{79}$$

The boundaries of the confidence interval of the Hill estimator are:

$$\widehat{\gamma}_{up,low} = \widehat{\gamma} \pm Q_N\widehat{V}_\gamma^{0.5}, \tag{80}$$

where Q_N is the quantile of a standard normal distribution corresponding to probability $0.5(1 + P_{\beta 1})$, whereas $P_{\beta 1} = \sqrt{P_\beta}$, while $P_\beta = 0.95$ is the confidence interval accepted for the entire estimate of the rate of exceedances – extrapolated estimate still needs to be multiplied by the estimate of rate of upcrossing the selected threshold.

The boundaries of the confidence interval of the extrapolated esti-

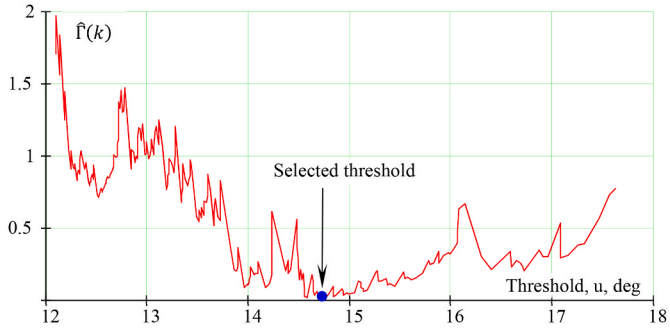

Fig. 12. Selecting a threshold with prediction error criterion for the data set 1.

Table 4
Heavy tail fitting results.

Data set	Selected threshold, deg.	Number of data points above the threshold	Hill estimator
1	14.7	99	0.141
2	13.8	183	0.140
3	16.7	38	0.107

mate are:

$$\widehat{P}(\phi > \phi^* | \phi > u)_{up,low} = \left(\frac{\phi^*}{u}\right)^{-\frac{1}{\widehat{\gamma}_{up,low}}}. \tag{81}$$

Numerical results of the calculation of the extrapolated estimates for all three data sets are presented in Table 5. The consistency of these estimates is noteworthy, especially as compared to the GPD extrapolation results summarized in Table 2.

The confidence interval for the threshold upcrossing rate is constructed from its binomial distribution with the parameter $\widehat{p}_U = \widehat{r}_U \Delta t$:

$$\begin{aligned} \widehat{r}_{U,low} &= Q_B\left(\frac{1 - P_{\beta 1}}{2}; \widehat{p}_U, k\right), \\ \widehat{r}_{U,up} &= Q_B\left(\frac{1 + P_{\beta 1}}{2}; \widehat{p}_U, k\right), \end{aligned} \tag{82}$$

where Q_B is a quantile of the binomial distribution corresponding to the probability $0.5(1 \pm P_{\beta 1})$, number of trials k and probability $\widehat{p}_U$.

Finally,

$$\begin{aligned} \widehat{r}_{\phi*,low} &= \widehat{r}_{U,low}\, \widehat{P}(\phi > \phi^* | \phi > u)_{low}, \\ \widehat{r}_{\phi*,up} &= \widehat{r}_{U,up}\, \widehat{P}(\phi > \phi^* | \phi > u)_{up}. \end{aligned} \tag{83}$$

The numerical results for all three data sets are shown in Fig. 13. When GPD was able to recover the positive shape parameter (data set 1), the heavy tail and GPD results are reasonably close. Both GPD and heavy tail extrapolation have captured the "true" value estimate from the full set of validation data (Campbell et al., 2023). GPD is slightly more conservative on the upper confidence interval boundary, as compared to the heavy tail. The difference in lower boundaries is more dramatic, but the lower boundary has a little practical importance.

A larger difference between the GPD and heavy tail extrapolation is observed for data set 2, where GPD shape parameter was estimated to be negative. The most probable GPD estimate is three orders of magnitude smaller than the "true" value, while the GPD mean value fares a bit better. The GPD upper boundary based on CDF has failed (5.7×10^{-7} 1/s $> 4.8 \times 10^{-7}$ 1/s), though the boundary method still worked due to its conservatism. The heavy tail extrapolation has recovered the "true" value from the same data set without any apparent problems. Finally, GPD extrapolation has completely failed on the data set 3, while the heavy-tail extrapolation exhibited a lower boundary but still has captured the "true" value within its confidence interval.

In general, the heavy tail extrapolation, when applicable, provides a more robust technique as compared to GPD. It also provides a substantial reduction in the width of the confidence interval. The latter is in line with the results of Glotzer et al. (2017) and supports the conclusions of the statistical validation effort described in Campbell et al. (2023).

Table 5
Results of heavy tail extrapolations.

Data set	Extrapolated estimate	Confidence interval	
		low	up
1	$8.27{\cdot}10^{-4}$	$1.06{\cdot}10^{-4}$	$3.05{\cdot}10^{-3}$
2	$5.10{\cdot}10^{-4}$	$1.14{\cdot}10^{-4}$	$1.50{\cdot}10^{-3}$
3	$2.78{\cdot}10^{-4}$	$2.162{\cdot}10^{-6}$	$24.5{\cdot}10^{-3}$

7. Summary

The current development of the Envelope Peak-over-Threshold (EPOT) technique application for the roll motion of a ship is summarized. EPOT is, essentially, a conventional Peak-Over-Threshold (POT) approach, where an envelope of the self-dependent data is applied to provide independent data. The Generalized Pareto Distribution (GPD) is a standard statistical model for approximating the tail of the distribution.

The application of the GPD to a practical volume of roll motion data may have issues, caused by natural variability of the shape parameter estimate. These issues may lead to an underestimation of an extrapolated estimate or an inability to complete the extrapolation due to the natural variability of the shape parameter estimate. The process of fitting the GPD tail is reviewed, and three numerical examples are considered: one, for which GPD works as expected, the second, when extrapolation nearly fails, and a third when it fails completely.

Analysis of the response of a reduced-order model (ROM) of roll motion with piecewise linear restoring leads to the conclusion that the shape parameter should be positive for large roll peaks. The paper reviews that solution and further examines the behavior of the shape parameter for relatively large samples of simulation data for ONR Tumblehome configuration at different headings. Complex tail structures were observed for stern quartering and beam seas, but the hypothesis of positive shape parameter was not rejected.

The physics-informed statistical model was formulated based on the hypothesis of positive shape parameter. The power-law/Pareto tail was used to model extremes of roll peaks. The paper addresses the selection of the threshold for the power-law tail with prediction error criterion and the construction of a confidence interval for the extrapolated estimates. Power law-tail calculations were performed for the same numerical examples and the results are compared with the GPD extrapolation.

8. Conclusions and future outlook

A physics-informed approach to extrapolation takes full advantage of the extreme value theory and augments it with application-specific physical information, improving robustness of the prediction and decreasing its statistical uncertainty. For a dynamical system with a softening nonlinearity in restoring, large peaks of roll motion are expected to have a power-law tail. The physical reason is that the softening nonlinearity makes a ship spend relatively more time at large roll angles near the maximum of the GZ curve. Including a requirement for a positive shape parameter into statistical model means using physics information – thus justifying the name of approach.

Two caveats are worth mentioning. The first is that the subject of these studies was the ONR Topside Series tumblehome configuration, which is known for its significant stability variation in following and stern-quartering seas. It would be beneficial to extend the study to other hull forms.

The second caveat is that complex structure of the distribution tail of roll peaks was observed. This complex structure is likely driven by the influence of other degrees of freedom and by stability variation in waves. To test this hypothesis, it would be beneficial to find out what phenomena form the tail structures. The tail structure for the bow seas heading remain unknown due to insufficient data. Resolving these caveats will help to extend and improve physics-informed statistical models of roll motions and should be considered for future research.

CRediT authorship contribution statement

Bradley Campbell: Conceptualization, Methodology, Investigation, Software, Writing – review & editing. **Vadim Belenky:** Conceptualization, Methodology, Investigation, Formal analysis, Data curation, Writing – original draft. **Vladas Pipiras:** Methodology, Investigation,

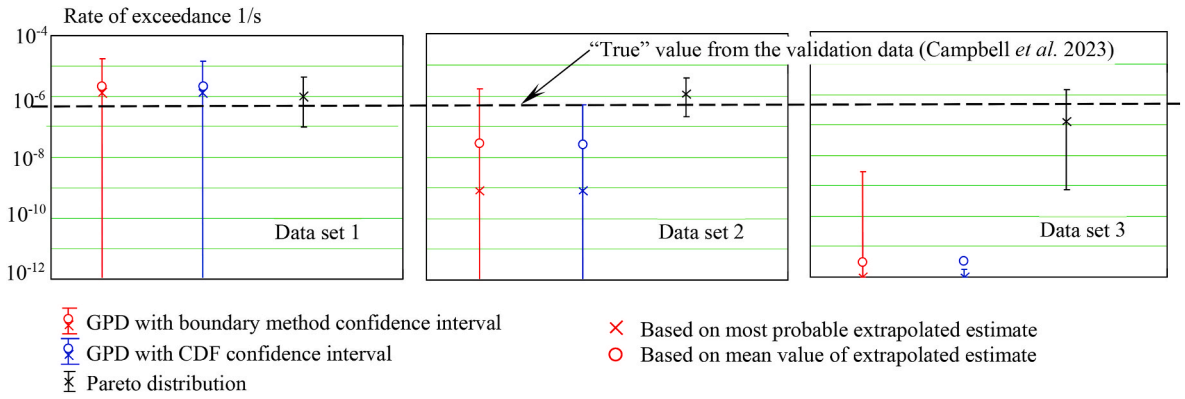

Fig. 13. Comparison of the results of extrapolation of the rate of exceedance of the target value $\varphi^* = 40$ deg. The "true" value from the validation data (Campbell et al., 2023) is 5.7×10^{-7} 1/s.

Formal analysis, Writing – review & editing. **Kenneth Weems:** Investigation, Methodology, Software, Validation, Data curation, Writing – review & editing. **Themistoklis P. Sapsis:** Methodology, Investigation, Formal analysis, Writing – review & editing.

Declaration of competing interest

The authors declare that they have no known competing financial interests or personal relationships that could have appeared to influence the work reported in this paper.

Data availability

Data will be made available on request.

Acknowledgements

The work described in this paper has been funded by the Office of Naval Research (ONR) under Dr. Woei-Min Lin and by the Naval Surface Warfare Center Carderock Division (NSWCCD) Independent Applied Research (IAR) program under Dr. Jack Price. The participation of Prof. Sapsis was facilitated by the NSWCCD Summer Faculty Program, while the participation of Prof. Pipiras was facilitated by NSWCCD Summer Faculty and Sabbatical Programs, both of which are managed by Dr. Jack Price. The authors are very grateful for the support that made this work possible.

References

Anastopoulos, P.A., Spyrou, K., 2023. Effectiveness of the generalized Pareto distribution for characterizing ship tendency for capsize. In: Spyrou, K., Belenky, V., Katayama, T., Bačkalov, I., Francescutto, A. (Eds.), Contemporary Ideas on Ship Stability – from Dynamics to Criteria, Springer Series Fluid Mechanics and its Application. ISBN 978-3-031-16328-9.

Beirlant, J., Goegebeur, Y., Teugels, J., Segers, J., 2004. Statistics of extremes, Wiley series in probability and statistics. In: Chichester, Theory and Applications, with Contributions from Daniel De Waal and Chris Ferro. John Wiley & Sons, Ltd.

Belenky, V.L., 2000. Piecewise linear approach to nonlinear ship dynamics. In: Vassalos, D., Hamamoto, M., Papanikolaou, A., Molyneux, D. (Eds.), Contemporary Ideas on Ship Stability". Elsevier, pp. 149–160. ISBN 0-08-043652-8.

Belenky, V.L., Sevastianov, N.B., 2007. Stability and Safety of Ships: Risk of Capsizing. Second edition SNAME, Jersey City. ISBN 0-939773-61-9.

Belenky, V., Weems, K.M., Bassler, C.C., Dipper, M.J., Campbell, B., Spyrou, K., 2012. Approaches to rare events in stochastic dynamics of ships. Probabilist. Eng. Mech. 28, 30–38.

Belenky, V., Campbell, B., 2012. Statistical Extrapolation for Direct Stability Assessment", *Proc. 11th Intl. Conf. On Stability of Ships And Ocean Vehicles*. STAB 2012), Athens, Greece, pp. 243–256.

Belenky, V., Weems, K., Pipiras, V., Glotzer, D., Sapsis, T., 2018. Tail structure of roll and metric of capsizing in irregular waves. In: Proc. 32nd Symp. Naval Hydrodynamics, Hamburg, Germany.

Belenky, V., Glotzer, D., Pipiras, V., Sapsis, T., 2019. Distribution tail structure and extreme value analysis of constrained piecewise linear oscillators. Probabilist. Eng. Mech. 57, 1–13.

Belenky, V., Weems, K., Lin, W.M., Pipiras, V., Sapsis, T., 2023. Estimation of Probability of Capsizing with Split-Time Method" *Ocean Engineering*, This issue.

Belknap, W.F., Reed, A.M., 2019. In: Belenky, V., Spyrou, K., van Walree, F., Neves, M.A. S., Umeda, N. (Eds.), TEMPEST: A New Computationally Efficient Dynamic Stability Prediction Tool" Chapter 1 of *Contemporary Ideas on Ship Stability. Risk of Capsizing*. Springer, pp. 3–21. ISBN 978-3-030-00514-6.

Bishop, R.C., Belknap, W., Turner, C., Simon, B., Kim, J.H., 2005. "Parametric Investigation on the Influence of GM, Roll Damping, and Above-Water Form on the Roll Response of Model 5613". Hydromechanics Department, Naval Surface Warfare Center Carderock Division, West Bethesda, Maryland, USA. Report NSWCCD-50-TR-2005/027.

Bretschneider, C.L., 1959. "Wave Variability and Wave Spectra for Wind-Generated Gravity Waves". U. S. Army Beach Erosion Board, Washington, DC, USA. Technical Memorandum 118.

Campbell, B., Belenky, V., 2010. "Assessment of Short-Term Risk with Monte-Carlo Method". Proc. 11th Intl. Ship Stability Workshop, Wageningen, the Netherlands, pp. 85–92.

Campbell, B., Belenky, V., 2010a. Statistical extrapolation for evaluation of probability of large roll. In: Proc. 11th Int. Symp. On Practical Design of Ships and Other Floating Structures PRADS 2010, pp. 436–446. Rio-de-Janeiro, Brazil.

Campbell, B., Belenky, V., Pipiras, V., 2014. On the application of the generalized Pareto distribution for statistical extrapolation in the assessment of dynamic stability in irregular waves. In: Proc. 14th Intl. Ship Stability Workshop. Kuala Lumpur, Malaysia, pp. 149–153.

Campbell, B., Belenky, V., Pipiras, V., 2015. In: Deodatis, G., Spanos, P.D. (Eds.), Properties of the Tail of Envelope Peaks and Their Use for the Prediction of the Probability of Exceedance for Ship Motions in Irregular Waves", *Proc. 7th Intl. Conf. Computational Stochastic Mechanics (CSM 7)*. https://doi.org/10.3850/978-981-09-5348-5_012. ISBN: 978-981-09-5347-8.

Campbell, B., Belenky, V., Pipiras, V., 2016. Application of the envelope peaks over threshold (EPOT) method for probabilistic assessment of dynamic stability. Ocean. Eng. 120, 298–304.

Campbell, B., Weems, K., Belenky, V., Pipiras, V., Sapsis, T., 2023. Envelope peaks over threshold (EPOT) application and verification. In: Spyrou, K., Belenky, V., Katayama, T., Bačkalov, I., Francescutto, A. (Eds.), Contemporary Ideas on Ship Stability – from Dynamics to Criteria. Springer, pp. 265–289. ISBN 978-3-031-16328-9.

Coles, S., 2001. An Introduction to Statistical Modeling of Extreme Values. Springer, London. ISBN 1-85233-459-2.

David, H.A., Nagaraja, H.N., 2005. Order Statistics, third ed. Wiley Series in Probability and Statistics. ISBN 978-0-471-72216-8.

Dupuis, D.J., Victoria-Feser, M.-P., 2006. A robust prediction error criterion for Pareto modelling of upper tails. Can. J. Stat. 34, 639–658.

Embrechts, P., Klüppelberg, C., Mikosch, T., 2013. Modelling Extremal Events: for Insurance and Finance. Springer Science & Business Media.

Glotzer, D., Pipiras, V., Belenky, V., Campbell, B., Smith, T., 2017. Confidence interval for exceedance probabilities with application to extreme ship motions. REVSTAT Stat. J. 15 (4), 537–563.

IMO MSC.1/Circ.1627 Interim Guidelines on the Second Generation Intact Stability Criteria, 2020. London, December.

Kim, D.H., Belenky, V., Campbell, B.L., Troesch, A.W., 2014. Statistical estimation of extreme roll in head seas. In: Proc. Of 33rd Intl. Conf. on Ocean, Offshore and Arctic Engineering. OMAE 2014, San-Francisco, USA.

Leadbetter, M.R., Lindgren, G., Rootzen, H., 1983. Extremes and Related Properties of Random Sequences and Processes, Springer Series in Statistics. Springer-Verlag, New York-Berlin. ISBN 978-0-387-90731-4.

Mager, J., 2015. Automatic Threshold Selection of the Peaks over Threshold Method. Master's Thesis, Technische Universität München. Germany. https://mediatum.ub.tum.de/doc/1254349/document.pdf.

Maki, A., 2017. Estimation method of the capsizing probability in irregular beam seas using non-Gaussian probability density function. J. Mar. Sci. Technol. 22 (2), 351–360.

Mohamad, M., Cousins, W., Sapsis, T., 2016. A probabilistic decomposition-synthesis method for the quantification of rare events due to internal instabilities. J. Comput. Phys. 322, 288–308.
Pickands, J., 1975. Statistical inference using extreme order statistics. Ann. Stat. 3 (1), 119–131.
Pipiras, V., 2020. Pitfalls of Data-Driven Peaks-Over-Threshold Analysis: Perspectives from Extreme Ship Motions, vol. 60. Probabilistic Engineering Mechanics, 103053.
Rosin, P., Rammler, E., 1933. The laws governing the fineness of powdered coal. J. Inst. Fuel 7, 29–36.
Ross, S.M., 1997. A First Course in Probability, fifth ed. Prentice Hull, Upper Saddle River, p. 514. ISBN 978-0-13-746314-5.
Shin, Y.S., Belenky, V.L., Lin, W.M., Weems, K.M., Engle, A.H., 2003. Nonlinear time domain simulation technology for seakeeping and wave-load analysis for modern ship design. SNAME Trans. 111, 557–578.
Smith, T.C., 2019. In: Belenky, V., Neves, M., Spyrou, K., Umeda, N., van Walree, F. (Eds.), Validation Approach for Statistical Extrapolation", Chapter 34 of *Contemporary Ideas on Ship Stability. Risk of Capsizing*. Springer, pp. 573–589, 2019 ISBN 978-3-030-00514-6.
Walpole, R.E., Myers, R.H., Myers, S.H., Ye, K., 2012. In: Probability and Statistics for Engineers and Scientists, ninth ed. Prentice Hall, Boston. ISBN-978-0-321-62911-1.
Weems, K., Belenky, V., Campbell, B., Pipiras, V., Sapsis, T., 2019. Envelope peaks over threshold (EPOT) application and verification. In: Proc. 17th Intl. Ship Stability Workshop, pp. 71–79. Helsinki, Finland.
Wandji, C., Shigunov, V., Pipiras, V., Belenky, V., 2024. Benchmarking of direct counting approaches. In: *Ocean Engineering,* This issue.
Weems, K., Belenky, V., 2015. Fast time-domain simulation in irregular waves with volume-based calculations for froude-krylov and hydrostatic force. In: Proc. 12th Intl. Conf. On Stability of Ships and Ocean Vehicles. STAB 2015), Glasgow, UK, pp. 891–901.
Weems, K., Belenky, V., 2023. Volume-base reduced-order model for ship motions. In: *Ocean Engineering,* This issue, 116214.
Weems, K., Wundrow, D., 2013. Hybrid models for fast time-domain simulation of stability failures in irregular waves with volume-based calculations for froude-krylov and hydrostatic force. In: Proc. Of 13th Intl. Ship Stability Workshop, pp. 130–137. Brest, France.